

A Photoelectrochemical Model of Proton Exchange Water Electrolysis for Hydrogen Production

Jianhu Nie

Yitung Chen

Robert F. Boehm

Shanthi Katukota

Department of Mechanical Engineering,
University of Nevada, Las Vegas,
Las Vegas, Nevada 89154

A photoelectrochemical model for hydrogen production from water electrolysis using proton exchange membrane is proposed based on Butler-Volmer kinetics for electrodes and transport resistance in the polymer electrolyte. An equivalent electrical circuit analogy is proposed for the sequential kinetic and transport resistances. The model provides a relation between the applied terminal voltage of electrolysis cell and the current density in terms of Nernst potential, exchange current densities, and conductivity of polymer electrolyte. Effects of temperature on the voltage, power supply, and hydrogen production are examined with the developed model. Increasing temperature will reduce the required power supply and increase the hydrogen production. An increase of about 11% is achieved by varying the temperature from 30°C to 80°C. The required power supply decreases as the illumination intensity becomes greater. The power supply due to the cathode overpotential does not change too much with the illumination intensity. Effects of the illumination intensity can be observed as the current density is relatively small for the examined illumination intensities. [DOI: 10.1115/1.2789722]

Keywords: photoelectrochemical model, electrolysis, PEM, hydrogen production

1 Introduction

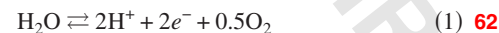
Hydrogen is expected to play an important role as an energy carrier of the future as the quality of human life increasingly depends on the availability of energy resources [1,2]. Hydrogen may be used as fuel in almost every application where fossil fuels are being used today, but almost without harmful emissions. However, hydrogen is not an energy source, and it does not occur in nature in its elemental or molecular form. Several methods have been and are being developed for production of hydrogen from renewable energy sources [3]. One of these methods is to capture the energy that is freely available from sunlight and to directly generate hydrogen. Research of photoelectrochemical systems that produce hydrogen directly from water using sunlight as the energy source has received increasing attention for the past decades [4,5]. Moreover, the advent of nanocrystalline semiconductor systems has rekindled interest in hydrogen production from water electrolysis by visible light [6].

The water electrolyzer cell with proton exchange membrane (PEM) has been utilized in many energy-related fields such as fuel cell, and solar cell systems. Electrolysis of water using the PEM is considered as a promising methodology for producing hydrogen because of its advantages over the classical alkaline process in terms of its simplicity, high energy efficiency, and specific production capacity. Basically, a PEM electrolyzer cell is similar to a PEM fuel cell. It has a polymer membrane, porous electrodes, current collectors and separator plates, end plates, bus plates, and manifolds. In general, the principle of operation is just reverse of fuel cell operation. On one electrode (anode), water is split into oxygen, protons, and electrons by applying a dc voltage higher than a thermoneutral voltage. Protons pass through the polymer electrolyte membrane and on the other electrode (cathode) combine with electrons to form hydrogen. Passage of protons through

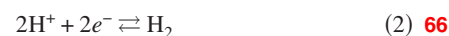
the membrane is accompanied by water transport (electro-osmotic drag). Although there are many studies on the theoretical analysis of PEM fuel cells [7–10], not much has been reported on the kinetics and polarization characteristics of the PEM electrolyzer cell. In order to design and use the PEM electrolyzer effectively, analytical and/or numerical models for the device are necessary so that the system may be optimized. Onda et al. [11] provided a voltage-current relation wherein the cell voltage is described as the sum of Nernst voltage, anode and cathode overpotentials, and resistive overpotential. Empirical equations were utilized for the anode and cathode overpotentials as a function of temperature of the electrolytes and current density of the cell. A simple model for electrochemical process in the water electrolysis cell was developed by Choi et al. [12]. However, none of such models, to the authors' knowledge, has been seen in the published literature for the photoelectrochemical PEM electrolysis cell. The present study is motivated by such need to develop a simple but useful first-generation theoretical model to explain the current-potential characteristics of photoelectrochemical PEM electrolysis cell based on the involved charge and mass balances as well as Butler-Volmer kinetics on the electrode surfaces.

Method Descriptions

Electrolysis of water is the dissociation of water molecules into hydrogen and oxygen. A potential is applied across the electrochemical cell to induce electrochemical reactions at both electrodes. A schematic of the water electrolysis cell is shown in Fig. 1. Water is introduced at the anode and dissociated into oxygen, protons, and electrons. For the pure water electrolysis process, the reaction at the anode can be expressed as



Under an electric field, the protons are driven through the PEM to the cathode where they combine with the electrons arriving from the external circuit to form hydrogen gas:



Contributed by the Heat Transfer Division of ASME for publication in the JOURNAL OF HEAT TRANSFER. Manuscript received January 26, 2007; final manuscript received March 28, 2007; published online xxxxx-xxxxx-xxxxx. Review conducted by Christopher Dames.

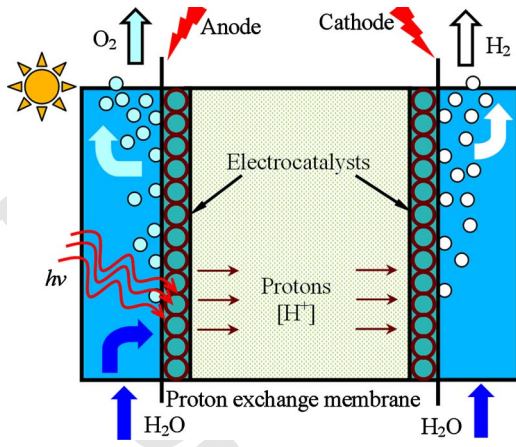


Fig. 1 Schematic of the PEM solar electrolyzer

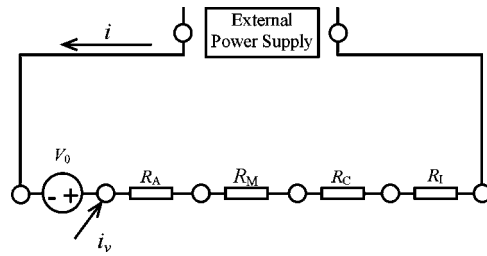


Fig. 2 Equivalent circuit for the solar water electrolysis process

Therefore, the net reaction in the electrolysis cell can be written as



The membrane-electrode assembly (MEA) is the main part of the PEM water electrolysis cell. The perfluorosulfonic acid polymer such as Nafion has been widely used as the membrane for water electrolysis because of its intrinsic properties: excellent chemical and mechanical stability, high protonic conductivity, and gas impermeability [13,14]. Because of the highly acidic environment produced by sulfonic acid groups at the membrane surfaces, acid-resistance noble metals or their oxides must be used for electrocatalysts. Platinum provides a significant overpotential and the best performance, and it is commonly used for water electrolysis [14].

Before a detailed analysis of the current distributions in the PEM electrolysis cell, it is important to have a correct description of the constituents of the cell voltage at the macroscopic level. A simplified mathematical model is developed based on appropriate mass balances, transport, and electrochemical kinetics applied to the PEM electrolysis cell, using the similar model development as Ref. [12].

First, the anode chamber is assumed to be well mixed. The mass balances of water and oxygen at the anode and that of hydrogen at the cathode can be written as [15]

$$\dot{N}_{\text{H}_2\text{O},\text{in}} - \dot{N}_{\text{H}_2\text{O},\text{out}} = \frac{iA}{2F} \quad (4)$$

$$\dot{N}_{\text{H}_2,\text{in}} - \dot{N}_{\text{H}_2,\text{out}} = -\frac{iA}{2F} \quad (5)$$

$$\dot{N}_{\text{O}_2,\text{in}} - \dot{N}_{\text{O}_2,\text{out}} = -\frac{iA}{4F} \quad (6)$$

where \dot{N} , i , A , and F are the molar flow rates, current density, MEA area, and Faraday constant, respectively.

The potential of the electrode when a net current flows through the electrode ($i \neq 0$) diminished by the equilibrium potential (when $i=0$) is called the overpotential. The overpotential may be regarded as the extra potential necessary to reduce the energy barrier of the rate-determining step to a value such that the electrode reaction proceeds at a desired rate. The stoichiometric number of a reaction is defined as the number of times the rate-determining step takes place for one act of overall reaction. The effect of light on electrode reactions is akin to its effect on chemical reactions (photochemistry). The number of electrons, n_ν , emitted in a second by a metal in a vacuum per unit of incident light energy is given by [16]

$$n_\nu = \frac{mc^2}{h^2\nu^2} \left(1 - \frac{\phi_M}{h\nu} \right) \quad (7)$$

where m is the mass of electron, c is the velocity of light, ϕ_M is the work function of the metal, and ν is the frequency of light of standard intensity I_0 .

It is assumed that there are no transport limitations. The Butler-Volmer expression utilized for the overall electrochemical reaction at the anode and the charge-transfer reaction under illumination can be given as [17]

$$i = i_{A0} \left[\exp\left(\frac{\alpha_A \nu_e^- F \eta_A}{RT}\right) - \exp\left(-\frac{(1-\alpha_A) \nu_e^- F \eta_A}{RT}\right) \right] + F \frac{I_\nu mc^2}{I_0 h^2 \nu^2} \left(1 - \frac{\phi_M + \chi}{h\nu} \right) \quad (8)$$

where i_{A0} is the anode exchange current density, ν_e^- is the stoichiometric coefficient of electrons in the anode, α_A is the transfer coefficient, η_A is the anode overpotential, I_ν is the intensity of illumination, R is the universal constant of gases, T is the temperature, and χ is the surface potential difference at the metal-solution surface.

Assuming that the effective transfer coefficient $\alpha_A=0.5$ and $\nu_e^-=2$ [18], the anode overpotential can be written in the following form:

$$i = i_{A0} \left[\exp\left(\frac{F \eta_A}{RT}\right) - \exp\left(-\frac{F \eta_A}{RT}\right) \right] + i_\nu \quad (9)$$

$$\eta_A = \frac{RT}{F} \sinh^{-1} \left(\frac{i - i_\nu}{2i_{A0}} \right) \quad (10)$$

where

$$i_\nu = F \frac{I_\nu mc^2}{I_0 h^2 \nu^2} \left(1 - \frac{\phi_M + \chi}{h\nu} \right) \quad (10)$$

Similarly, for the cathode, if Butler-Volmer equation is utilized along with $\alpha_C=0.5$ and $\nu_e^--=2$, the cathode overpotential can be obtained as

$$\eta_C = -\frac{RT}{F} \sinh^{-1} \left(\frac{i_C}{2i_{C0}} \right) \quad (11)$$

where i_{C0} is the cathode exchange current density. Here, it should be noted that the solutions are assumed to be well mixed in the chambers and thus the surface concentrations do not differ appreciably from the bulk phase.

At steady state, the divergence of current density in the PEM is zero, i.e.,

$$\frac{di}{dz} = 0 \quad \text{and} \quad i = -\sigma \frac{d\phi}{dz} \quad (12)$$

where σ is the conductivity of the electrolyte and ϕ is the potential in the membrane.

Figure 2 shows the equivalent circuit for photoelectrolysis pro-

cess represented by a series of resistances. The overall applied cell potential is thus composed of the cell Nernst potential (V_0), anode (η_A) and cathode (η_C) overpotentials, overpotential due to membrane (η_M), and interfacial resistance (η_I). It can be written as

$$V = V_0 + \eta_A - \eta_C + \eta_M + \eta_I \quad (13)$$

where the interfacial overpotential (η_I) may be written in terms of interfacial resistance R_I and current density as $\eta_I = R_I i$.

The Nernst potential or equilibrium open circuit potential (V_0) is empirically expressed as [19]

$$V_0 = \frac{\Delta G}{2F} + \frac{\Delta S}{2F}(T - T_{ref}) + \frac{RT}{2F} \left[\ln(P_{H_2}) + \frac{1}{2} \ln(P_{O_2}) \right] \quad (14)$$

From the reaction as shown in Eqs. (1)–(3), the equilibrium potential can be expressed as

$$V_0 = 1.23 - 0.9 \times 10^{-3}(T - 298) + \frac{RT}{4F} \ln(P_{H_2}^2 P_{O_2}) \quad (15)$$

The overpotential due to membrane resistance can be obtained by integrating Eq. (12):

$$\eta_M = \left(\frac{L_M}{\sigma_M} \right) i \quad (16)$$

where L_M is the thickness of the PEM, and σ_M is the conductivity of the electrolyte. The membrane's resistance depends mainly on the temperature and moisture content in the membrane. Conductivity of Nafion can be described by the following relation [20]:

$$\sigma_M = \sigma_M^{ref} \exp \left[1268 \left(\frac{1}{T_{ref}} - \frac{1}{T} \right) \right] \quad (17)$$

Therefore, the overall cell voltage-current relation for the electrolysis cell can be obtained by combining the above equations:

$$V = V_0 + \frac{RT}{F} \sinh^{-1} \left[\frac{1}{2} \left(\frac{i - i_v}{i_{A0}} \right) \right] + \frac{RT}{F} \sinh^{-1} \left[\frac{1}{2} \left(\frac{i_C}{i_{C0}} \right) \right] + \left(\frac{L_M}{\sigma_M} \right) i + R_I i \quad (18)$$

Then, the required power density can be obtained by $P = Vi$ as

$$P = V_0 i + \frac{RT}{F} \sinh^{-1} \left[\frac{1}{2} \left(\frac{i - i_v}{i_{A0}} \right) \right] i + \frac{RT}{F} \sinh^{-1} \left[\frac{1}{2} \left(\frac{i_C}{i_{C0}} \right) \right] i + \left(\frac{L_M}{\sigma_M} \right) i^2 + R_I i^2 \quad (19)$$

The rate of hydrogen production is derived in a way similar to hydrogen usage in the PEM fuel cell, except that there are two moles of electrons to generate a mole of hydrogen, and hence the hydrogen production rate is written as follows:

$$H_{2,production} = \frac{i}{2F} \quad (20)$$

The electrolysis process has been represented by an equivalent electrical circuit consisting of a series of resistances standing for each individual steps. In analogy to linear Ohm's law, a differential resistance R_d can be defined for an electrolysis cell as [18]

$$R_d = \frac{d(V - V_0)}{di} \quad (21)$$

$$R_d = \frac{d\eta_A}{di} - \frac{d\eta_C}{di} + \frac{d\eta_M}{di} + \frac{d\eta_I}{di} = R_A + R_C + R_M + R_I \quad (22)$$

$$R_A = \frac{RT}{(2Fi_{A0})\sqrt{1 + ((i - i_v)/2i_{A0})^2}} \quad (23)$$

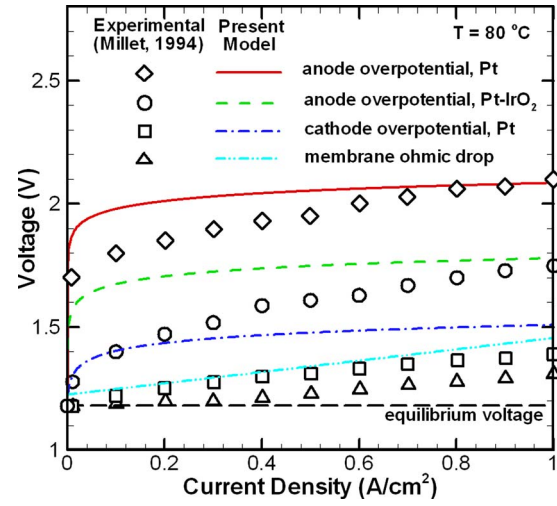


Fig. 3 Comparisons of the computed results with the measured data

$$R_C = \frac{RT}{(2Fi_{C0})\sqrt{1 + (i_C/2i_{C0})^2}} \quad (24)$$

$$R_M = L_M/\sigma_M \quad (25)$$

It should be noted that $i_C = i - i_v$.

Results and Discussions

The voltage-current density curves are presented in Fig. 3 for pure water electrolysis (without photocurrent) at the temperature of $T = 80^\circ\text{C}$. Values of the physical properties are listed in Table 1. During the present modeling, the conductivity of the electrolyte at the reference state (σ_m^{ref}), which appears in Eq. (17), is determined to be 0.072 S/cm at the reference temperature of $T_{ref} = 298$ K. In addition, a correction factor of 1.75 from computer optimization is used in Eqs. (8) and (11), because there is a limitation for mass transfer, e.g., oxygen diffusion from catalyst site to gas bubble across a diffusion film near electrodes. Such value is selected as fitting parameter in order to optimize the match with the experimental data, as shown in Fig. 3. The exchange current density, i_0 , depends on the temperature at the electrode surface and also the roughness factor, which is defined as the electrochemically determined electrode area divided by the geometric area: $i_0 = \gamma_M \times \exp[-E/R((1/T) - (1/T_{ref}))] i_0^{ref}$, where E is the activation energy. It can be seen that comparisons between the computed results and the measured data [13] are in very favorable agreement.

Effects of different temperatures on the voltage-current density curves are shown in Fig. 4. The anode and cathode overpotentials are presented in Fig. 4(a) as a function of the current density. It can be seen that the anode and cathode overpotentials become greater as the temperature decreases, as a result of the decreasing exchange current density with the increase of temperature. For the purpose of clarity, the membrane Ohmic drop and the equilibrium voltage are exhibited in Fig. 4(b). Both the membrane Ohmic drop and the equilibrium voltage become greater as the temperature decreases.

Figure 5 shows the differential resistances for water electrolysis cell for different temperatures. The membrane differential resis-

Table 1 Model parameters for water electrolysis cell

Parameters	$i_{A0,Pt}$	$i_{A0,Pt-IrO_2}$	i_{C0}	L_M	γ_M
Values	10^{-9}	8×10^{-7}	3×10^{-3}	178	150
Dimensions	A/cm ²	A/cm ²	A/cm ²	μm	1

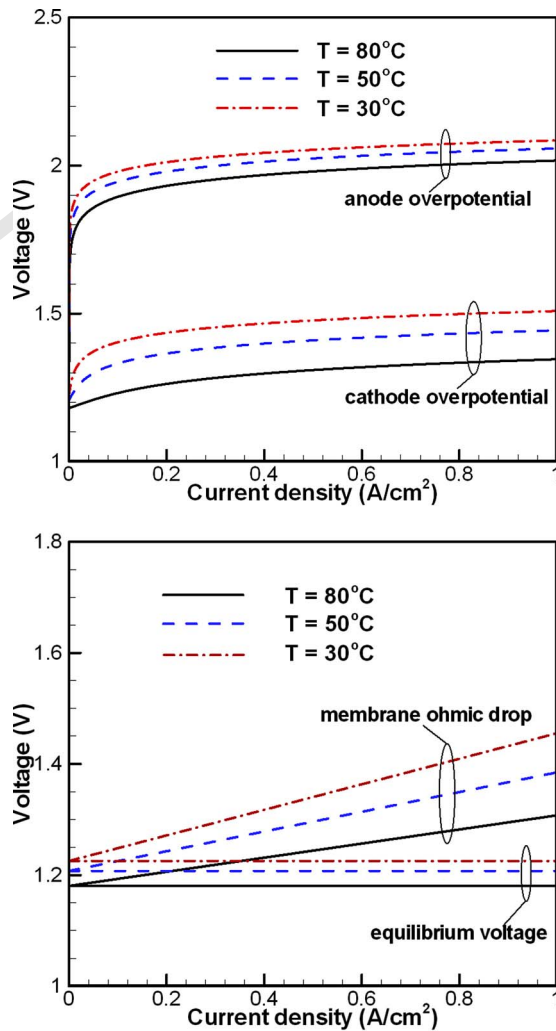


Fig. 4 Effects of temperature on the voltages of the water electrolysis cell

219 tance increases with the decrease of temperature. As the tempera-
 220 ture becomes smaller (such as $T=50^{\circ}\text{C}$ and 30°C), the anode and
 221 the cathode differential resistances become close to each other. At
 222 $T=30^{\circ}\text{C}$, they almost overlay with each other. Effects of tempera-
 223 ture on the power supply are presented in Fig. 6. The minimum
 224 power supply in this figure is the required power supply for over-
 225 coming the equilibrium open circuit potential. The required power
 226 supply increases as the temperature decreases. This can be seen
 227 more clearly for the power supply due to anode overpotentials.
 228 Hydrogen production rates for different temperatures are exhibited
 229 in Fig. 7. For the same power supply, the hydrogen production
 230 rate becomes greater with the increase of temperature. For in-
 231 stance, the hydrogen production rate increases by approximately
 232 11% from the temperature of 30°C to 80°C .

233 Effects of the illumination intensity on the voltage-current
 234 density curves are presented in Fig. 8 for $I_p/I_0=0, 0.5, \text{ and } 1$. The
 235 temperature is taken as a constant of $T=80^{\circ}\text{C}$. The frequency of
 236 the incident light is typically taken as 6.5×10^{15} Hz. The surface
 237 potential (χ) is assumed to be 0.1 eV, although different values
 238 can be examined without a lot of difficulties. Both the anode and
 239 the cathode overpotentials decrease as the illumination intensity
 240 increases. This can be seen more clearly as the magnitude of the
 241 current density is small. Effects of the illumination intensity be-
 242 come less significant as the current density increases. This is be-
 243 cause for the selected illumination intensities, the photocurrent
 244 plays a more important role than the electrochemical current. As

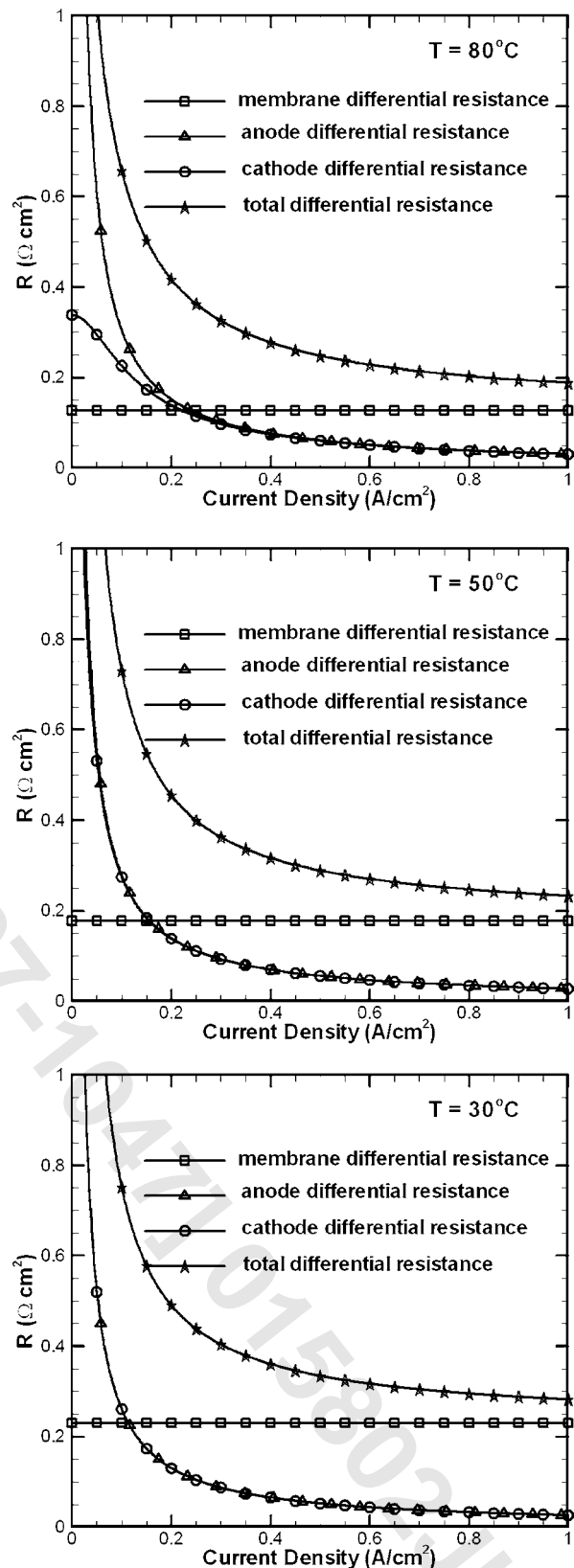


Fig. 5 Effects of temperature on differential resistances for water electrolysis

the current density increases, the electrochemical current becomes
 245 more predominant and then effects of the photocurrent become
 246 less significant. 247

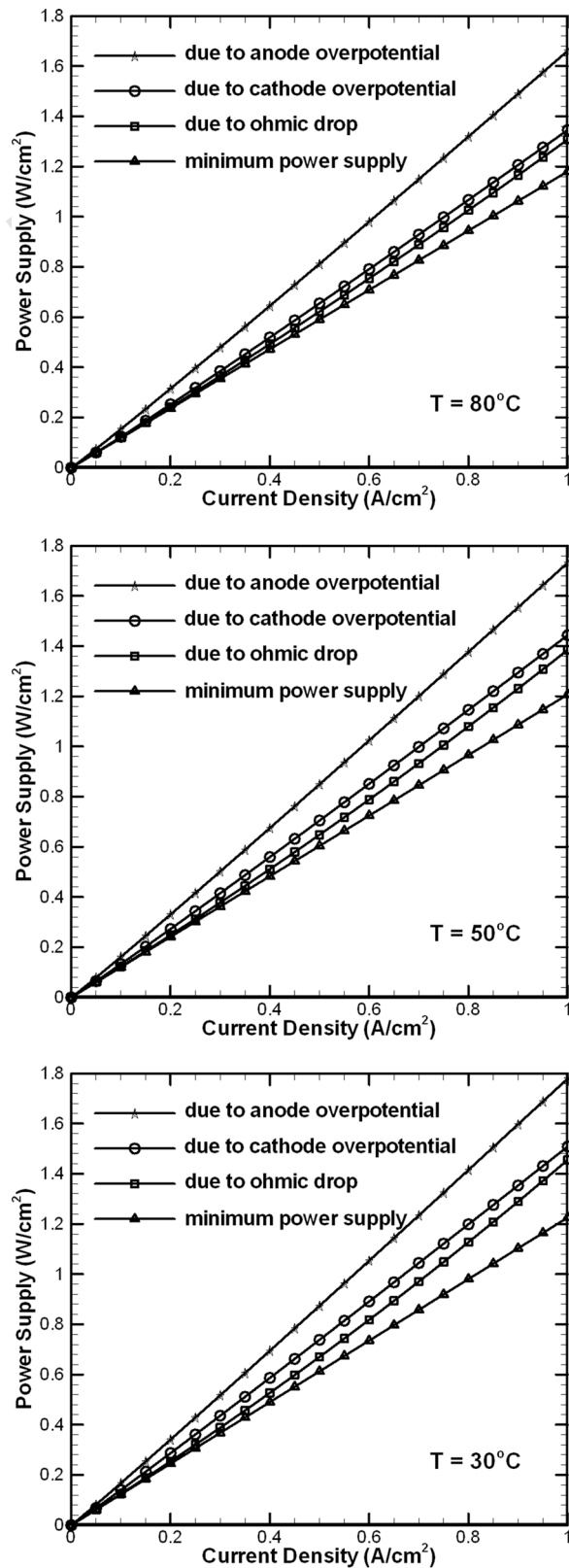


Fig. 6 Effects of temperature on required power supply for water electrolysis

248 The power supplies due to the anode and cathode overpotentials
 249 for different illumination intensities are plotted in Fig. 9. Effects
 250 of the illumination intensity can be observed as the current density
 251 is relatively small. The required power supply decreases as the

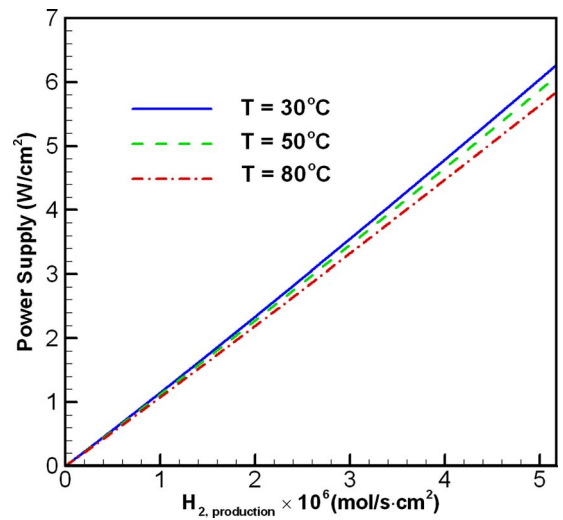


Fig. 7 Effects of temperature on hydrogen production rate

illumination intensity becomes greater. The power supply due to
 the cathode overpotential does not change too much with the illumina-
 tion intensity. Illumination intensity effects on the hydrogen
 production are presented in Fig. 10. Effects of the illumination
 intensity can be observed as the current density is relatively small
 for the examined illumination intensities.

Conclusions

A photoelectrochemical model is developed for the water elec-
 trolysis process. Electrolysis process is represented by the equiva-
 lent electric circuit. Effects of temperature on the voltage, power
 supply, and hydrogen production are examined with the developed
 model. Increasing temperature will decrease the required power
 supply and increase the hydrogen production. An increase of
 about 11% is achieved by varying the temperature from 30°C to
 80°C. The required power supply decreases as the illumina-
 tion intensity becomes greater. The power supply due to the
 cathode overpotential does not change too much with the illumina-
 tion intensity. Effects of the illumination intensity can be obser-
 ved as the current density is relatively small for the examined
 illumination intensities.

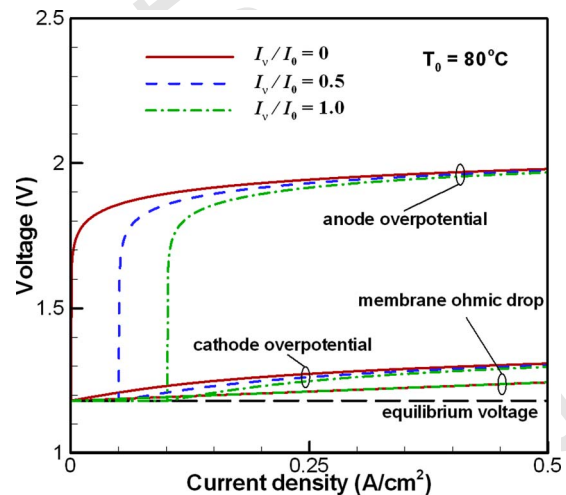


Fig. 8 Effects of illumination intensity on voltage-current density curve

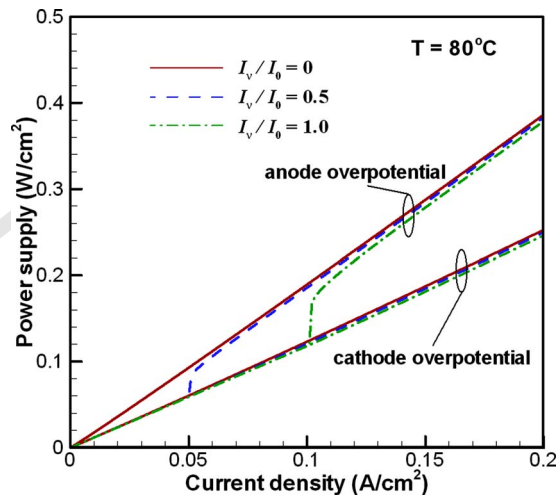


Fig. 9 Effects of illumination intensity on electrode overpotentials

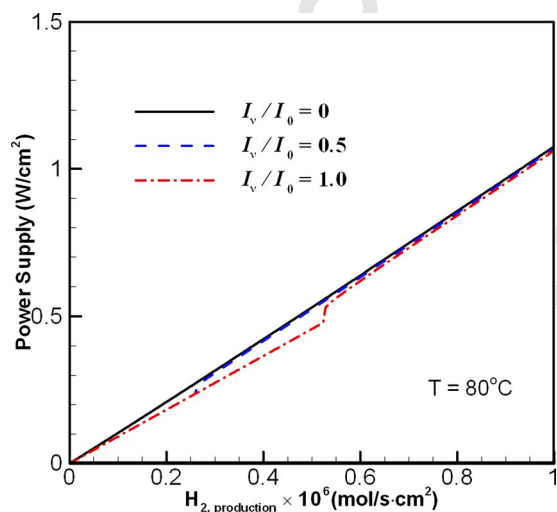


Fig. 10 Effects of illumination intensity on hydrogen production rate

272 Acknowledgment

273 This work was supported by US Department of Energy under
274 Grant Nos. DE-FG36-03GO13063 and RF-05-HFS-006. The use
275 of computer resources provided by the National Supercomputing
276 Center for Energy and the Environment is gratefully acknowl-
277 edged.

278 Nomenclature

- 280** c = speed of light in vacuum = 2.9979×10^8 m/s
- 281** E = activation energy
- 282** F = Faraday constant = 9.6485×10^4 C/mol
- 283** h = Planck constant = 6.626×10^{-34} J s
- 286** I_0 = standard intensity of light
- 287** i = current density
- 288** i_0 = exchange current density
- 289** L_B = thickness of the proton exchange membrane
- 290** m = mass of electron = 9.1096×10^{-31} kg
- 292** \dot{N} = molar flow rate
- 293** n = number of electrons transferred in the reaction

- P = pressure **294**
- R = universal constant of gases = 8.314 J/(mol K) **296**
- R_A = anode differential resistance **297**
- R_C = cathode differential resistance **298**
- R_I = interfacial differential resistance **299**
- R_M = membrane differential resistance **300**
- T = temperature **301**
- T_{ref} = reference temperature **302**
- V = voltage **303**
- V_0 = equilibrium voltage **304**

Greek Symbols

- α = transfer coefficient **306**
- χ = surface potential difference at the metal-solution interface **307**
- γ_M = roughness factor **308**
- σ_B = conductivity of the electrolyte **309**
- ϕ_M = work function of the metal **310**
- ν = frequency of light **311**
- η = overpotential **312**
- η_A = anode overpotential **313**
- η_C = cathode overpotential **314**
- η_I = overpotential due to interfacial resistance **315**
- η_M = overpotential due to membrane **316**

References

- [1] Adamson, K., 2004, "Hydrogen From Renewable Resources—The Hundred Year Commitment," *Energy Policy*, **32**(10), pp. 1231–1242. **319**
- [2] Ogden, J. M., 2002, "Hydrogen: The Fuel of the Future?" *Phys. Today*, **55**(4), pp. 69–75. **320**
- [3] Barbir, F., 2005, "PEM Electrolysis for Production of Hydrogen From Renewable Energy Sources," *Sol. Energy*, **78**(5), pp. 661–669. **321**
- [4] Nozik, A. J., 1978, "Photoelectrochemistry: Applications to Solar Energy Conversion," *Annu. Rev. Phys. Chem.*, **29**, pp. 189–222. **322**
- [5] Grätzel, M., 2001, "Photoelectrochemical Cells," *Nature (London)*, **414**(6861), pp. 338–344. **323**
- [6] Grätzel, M., 2005, "Mesoscopic Solar Cells for Electricity and Hydrogen Production From Sunlight," *Chem. Lett.*, **34**(1), pp. 8–13. **324**
- [7] Cheddie, D., and Munroe, N., 2005, "Review and Comparison of Approaches to Proton Exchange Membrane Fuel Cell Modeling," *J. Power Sources*, **147**(1–2), pp. 72–84. **325**
- [8] Scott, K., Taama, W., and Cruickshank, J., 1997, "Performance and Modeling of a Direct Methanol Solid Polymer Electrolyte Fuel Cell," *J. Power Sources*, **65**(1–2), pp. 159–171. **326**
- [9] Nguyen, T. V., and White, R. E., 1993, "A Water and Heat Management Model for Proton-Exchange-Membrane Fuel-Cells," *J. Electrochem. Soc.*, **140**(8), pp. 2178–2186. **327**
- [10] Larminie, J., and Dicks, A., 2000, *Fuel Cell Systems Explained*, Wiley, New York. **328**
- [11] Onda, K., Murakami, T., Hokosaka, T., Kobayashi, M., Notu, R., and Ito, K., 2002, "Performance Analysis of Polymer-Electrolyte Water Electrolysis Cell at a Small-Unit Test Cell and Performance Prediction of Large Stacked Cell," *J. Electrochem. Soc.*, **149**(8), pp. A1069–A1078. **329**
- [12] Choi, P., Bessarabov, D. G., and Datta, R., 2004, "A Simple Model for Solid Polymer Electrolyte (SPE) Water Electrolysis," *Solid State Ionics*, **175**(1–4), pp. 535–539. **330**
- [13] Millet, P., 1994, "Water Electrolysis Using EME Technology—Electric-Potential Distribution Inside a Nafion Membrane During Electrolysis," *Electrochim. Acta*, **39**(17), pp. 2501–2506. **331**
- [14] Ioroi, T., Yasuda, K., Siroma, Z., Fujiwara, N., and Miyazaki, Y., 2002, "Thin Film Electrocatalyst Layer for Unitized Regenerative Polymer Electrolyte Fuel Cells," *J. Power Sources*, **112**(2), pp. 583–587. **332**
- [15] Bard, A. J., and Faulkner, L. R., 2001, *Electrochemical Methods: Fundamentals and Applications*, 2nd ed., Wiley, New York. **333**
- [16] Wilson, H. A., 1959, *Modern Physics*, 4th ed., Blackie, London, Chap. 4. **334**
- [17] Bockris, J. O'M., 1954, in *Modern Aspects of Electrochemistry*, Bockris, J. O'M., and Conway, B. D., eds., Butterworth, London, vol. 1, Chap. 4. **335**
- [18] Bockris, J. O'M., and Srinivasan, S., 1969, *Fuel Cells: Their Electrochemistry*, McGraw-Hill, New York. **336**
- [19] Bernardi, D. M., and Verbrugge, M. W., 1992, "Mathematical Model of the Solid-Polymer-Electrolyte Fuel Cell," *J. Electrochem. Soc.*, **139**(9), pp. 2477–2491. **337**
- [20] Beattie, P. D., Basura, V. I., and Holdcroft, S., 1999, "Temperature and Pressure Dependence of O₂ Reduction at Pt | Nafion® 117 and Pt | BAM® 407 Interfaces," *J. Electroanal. Chem.*, **468**(2), pp. 180–192. **338**